Cell PRESS

Chemistry & Biology
Article

Targeting a Uniquely Nonspecific Prenyl Synthase with Bisphosphonates to Combat Cryptosporidiosis

Jennifer D. Artz,[1,8] James E. Dunford,[2,3,8] Michael J. Arrowood,[4,8] Aiping Dong,[1] Maksymilian Chruszcz,[5,6] Kathryn L. Kavanagh,[2] Wladek Minor,[5,6] R. Graham G. Russell,[3] F. Hal Ebetino,[7] Udo Oppermann,[2,3] and Raymond Hui[1,*]
[1]Structural Genomics Consortium, University of Toronto, 101 College Street, Toronto, ON M5G 1L7, Canada
[2]Structural Genomics Consortium, University of Oxford, Old Road Campus, Oxford OX3 7DQ, UK
[3]Institute of Musculoskeletal Sciences, University of Oxford, Nuffield Department of Orthopaedic Surgery, Botnar Research Centre, Headington, Oxford OX3 7LD, UK
[4]Centers for Disease Control and Prevention, Atlanta, GA 30333, USA
[5]Department of Molecular Physiology and Biological Physics, University of Virginia, Charlottesville, VA 22908-0736, USA
[6]Midwest Center for Structural Genomics
[7]Procter & Gamble Pharmaceuticals, Inc., Mason, OH 45040, USA
[8]These authors contributed equally to this work.
*Correspondence: Raymond.hui@utoronto.ca
DOI 10.1016/j.chembiol.2008.10.017

SUMMARY

Cryptosporidiosis is a neglected disease without a wholly effective drug. We present a study demonstrating nitrogen-containing bisphosphonates (N-BPs) to be capable of inhibiting *Cryptosporidium parvum* at low micromolar concentrations in infected MDCK cells. Predictably, the mechanism of action is based on inhibition of biosynthesis of isoprenoids but the target enzyme is unexpectedly a distinctive *C. parvum* enzyme dubbed nonspecific polyprenyl pyrophosphate synthase (CpNPPPS). This enzyme produces various isoprenoid products larger than FPP and is inhibited by N-BPs at subnanomolar concentrations. It is part of an isoprenoid pathway in *Cryptosporidium* distinctly different from other organisms. The proposed mechanism of action is corroborated by crystal structures of the enzyme with risedronate and zoledronate bound showing how this enzyme's unique chain length determinant region enables it to accommodate larger substrates and products. These results, combined with existing data on their clinical use, demonstrate that N-BPs are very promising anticryptosporidial drug candidates.

INTRODUCTION

Given their significant impact on global health, protozoan diseases do not benefit from a proportionate share of research support and are therefore often classified as neglected diseases. An example is cryptosporidiosis (Savioli et al., 2006), a potentially severe enteric disease primarily affecting pregnant women, immunocompromised individuals, and children. Millions of Asian and African children under 5 years of age suffer repeated infection and consequently intellectual stunting (Berkman et al., 2002; Ricci et al., 2006). In addition, *Cryptosporidium parvum* is a major cause of livestock infection and is classified as a class B bioterror agent.

The most common prescriptions for cryptosporidiosis are nitazoxanide and the antibiotic paromomycin, with the former approved for otherwise healthy adults and children older than 1 year of age (Smith and Corcoran, 2004). Neither is targeted therapy with known mechanism of action. In general, efforts to identify and validate *Cryptosporidium* drug targets are complicated by the parasite's resistance to genetic manipulation and long-term cultivation. Even with the establishment of a promising drug target, the traditional drug-discovery cycle that follows—including discovery and optimization of novel inhibitory compounds, ADME/toxicity assessment, and finally animal and clinical studies—is too long, expensive, and prone to failure for an infectious disease that requires a therapeutic solution sooner rather than later.

In lieu of developing novel drugs, revisiting known chemical space and investigating the efficacy of compound classes first developed for diseases other than cryptosporidiosis might prove to be highly efficient, particularly if such compounds have known favorable pharmacokinetic properties or, better still, are already in clinical use. For example, in vitro studies have shown nitrogen-containing bisphosphonates (N-BP), many of which are clinically approved for treatment of bone metabolism disorders, to be effective in killing bacterial pathogens such as *Staphylococcus aureus* (Liu et al., 2008) as well as other protozoan parasites including *Plasmodium*, *Toxoplasma*, *Leishmania*, and *Trypansoma* (Sanz-Rodriguez et al., 2007). Their utility on cryptosporidiosis has not been studied to the same extent; however, previous preliminary work has indicated that one member of the N-BP family is effective against experimental cryptosporidiosis in a mouse xenograft model (Moreno et al., 2001).

Clinically, N-BPs are widely used to treat bone metabolism disorders, such as osteoporosis (Delmas, 2002). In these treatments, N-BPs inhibit the isoprenoid pathway by binding to their molecular target, namely farnesyl pyrophosphate synthase (FPPS) (van Beek et al., 1999; Bergstrom et al., 2000; Fisher et al., 2000; Rogers et al., 2000; Dunford et al., 2001). Similarly, the isoprenoid pathway has been considered a drug target for protozoan diseases, including malaria, Chagas' disease, toxoplasmosis, and leishmaniasis (Ling et al., 2005; Martin et al., 2001; Moreno et al., 2001). In *C. parvum*, the importance of

 ©2008 Elsevier Ltd All rights reserved

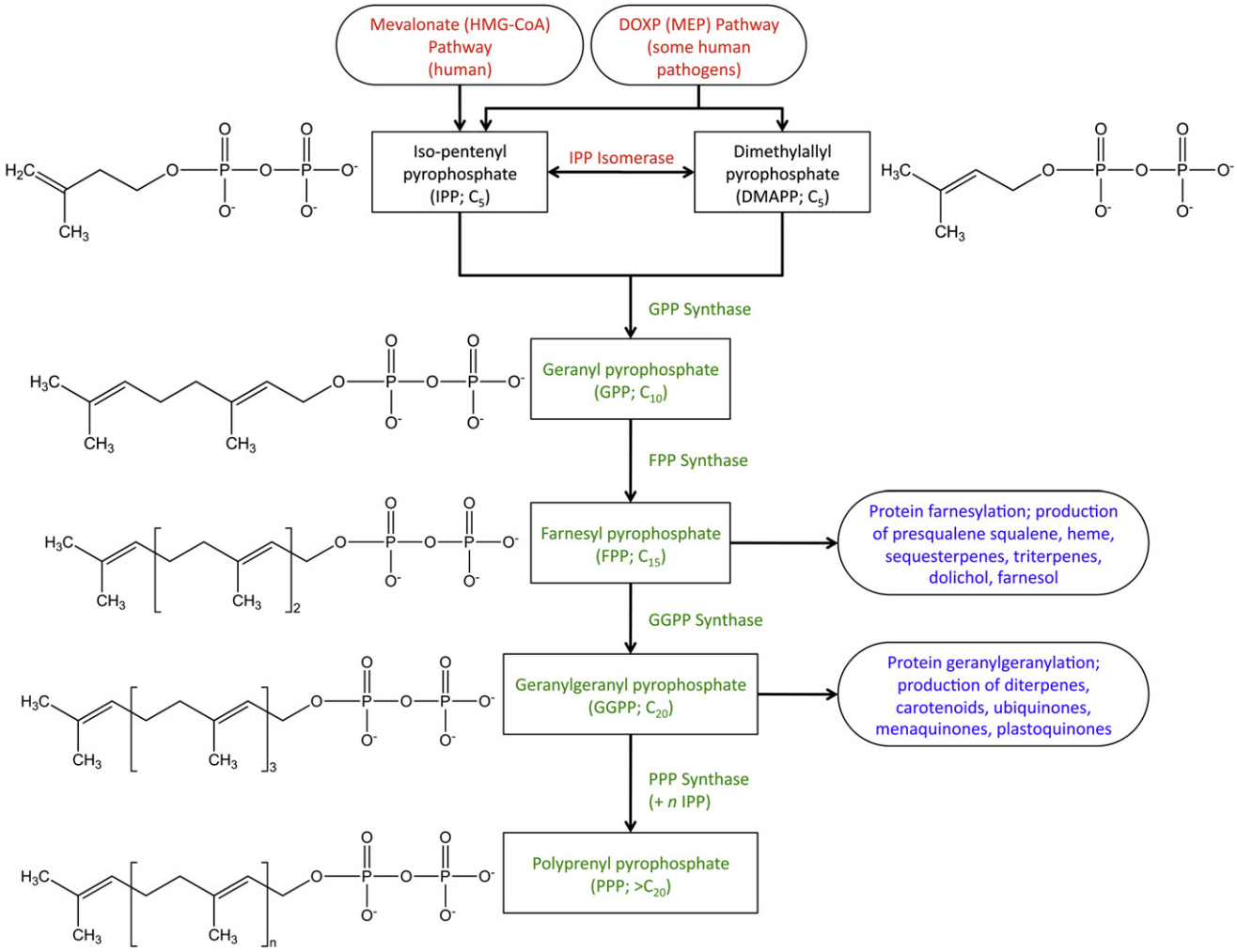

Figure 1. Isoprenoid Synthesis and Downstream Products

C. parvum enzyme activities (and respective products) that have been identified and characterized are in green (this work). The MVA pathway, used by most eukaryotes for producing IPP, is absent, as is the MEP pathway employed by prokaryotes and other protozoan parasites. From genomic analysis, however, there appear to be downstream enzymes that build on medium-length isoprenoids.

isoprenoids is supported by the prediction of at least three prenyl synthases in the genome (data not shown); however, unlike *Plasmodium* and *Toxoplasma* parasites, which employ the MEP pathway (Figure 1), the path leading to production of substrates for these enzymes, including isopentenyl pyrophosphate (IPP) and dimethylallyl pyrophosphate (DMAPP), is unclear, because the requisite enzymes have not been found by experiment or genomic analysis (Clastre et al., 2007). At this point, it is unknown whether the *Cryptosporidium* genus of parasites relies heavily on salvage or on a completely different pathway for isoprenoids.

In our study, we chose a panel of N-BPs to quantify their effectiveness in a MDCK (Madin Darby canine kidney) cell *Cryptosporidium* infection model. To investigate the mechanism of action, the *C. parvum* enzyme most closely homologous to FPPS and GGPPS was expressed and characterized by means of biochemical assays and crystallography. Our results revealed this enzyme to be a nonspecific polyprenyl pyrophosphate synthase (NPPPS) distinguished from all previously characterized enzymes in its unique capability to produce isoprenoid products from C_{20} to longer than C_{45}, depending on the substrate used. Structurally, it is similar to known orthologs of polyprenyl synthases including FPPS, GGPPS, and OPPS (octaprenyl pyrophosphate synthase) but reveals distinctive features consistent with its nonspecific substrate preference. Notwithstanding its novelty, CpNPPPS is efficiently inhibited by clinically relevant concentrations of N-BPs, and is therefore a potential target for the treatment of cryptosporidiosis.

RESULTS AND DISCUSSION

Inhibition of *C. parvum* Growth in MDCK Cell Culture by N-BPs

We screened a panel of seven clinically prescribed N-BPs against *C. parvum*-infected MDCK cell culture and analyzed the effect of the drugs by means of immunofluorescence labeling

Table 1. Anticryptosporidial Activity of N-BP Compounds in MDCK Cells

Compound	Structure	IC_{50} (μM)	*r*	TC_{50} MDCK Cells	TC_{50} HCT-8 Cells
IBAN	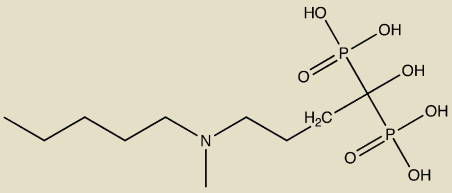	3.0	0.95	>100	>500
RIS	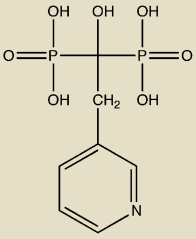	3.5	0.94	>100	>500
ZOL	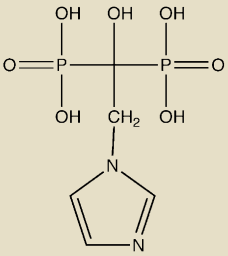	5.9	0.81	>100	>500
Pamidronate	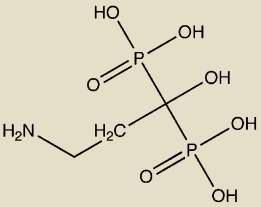	12.1	0.61	>100	>500
NE10790	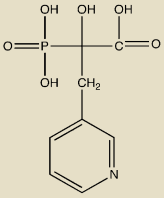	52.5	0.96	>100	>500
NE058051	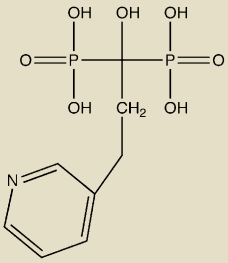	>100	0.89	>100	>500

 ©2008 Elsevier Ltd All rights reserved

Table 1. *Continued*

Compound	Structure	IC_{50} (μM)	*r*	TC_{50} MDCK Cells	TC_{50} HCT-8 Cells
Alendronate	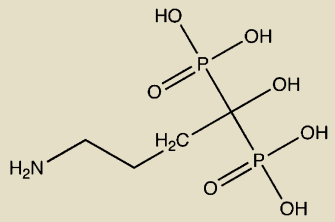	>100	0.28	>100	>500

IC_{50} represents 50% inhibitory concentration; r, linear correlation coefficient of median effect plot; TC_{50}, 50% inhibitory (toxicity) concentration.

of the monoclonal antibody C3C3 (see Experimental Procedures). Although both MDCK and HCT-8 cells support efficient (but not continuous) *Cryptosporidium* growth, MDCK cells were chosen for our experiments because they better facilitate digital imaging (Arrowood, 2007). As shown in Table 1, of the seven compounds, Alendronate and NE58051 showed negligible effect (IC_{50} > 100 μM). Pamidronate and NE10790 showed modest anticryptosporidial activity (IC_{50} ~12.1 and 52.3 μM, respectively) in the same order of magnitude as that of paromomycin, which is the standard for anticryptosporidial candidates (Perkins et al., 1998). Three candidates, namely risedronate (RIS), zoledronate (ZOL), and ibandronate (IBAN), showed the most promising activity (IC_{50} ~3 to 6 μM)—more than an order of magnitude stronger than the inhibitory potency of paromomycin and more potent than any other results cited in the literature, based on our survey. Because all seven compounds used showed low toxicity for MDCK up to 100 μM relative to control cells treated with medium alone (data not shown), these results indicate that the effective compounds entered the parasite and inhibited their development. As an illustrative example, Figure 2 shows the significantly inhibited growth in the presence of ZOL at 100 μM versus at 1 μM.

Activity Assays: Distinctive Cryptosporidium Enzyme Is the Target of Bisphosphonates

Bisphosphonates are known to inhibit the biosynthesis of isoprenoids, making this a good starting point for target identification; however, the *C. parvum* genome lacks the genes for both the MVA and MEP pathways for IPP production and is further missing isopentenyl pyrophosphate isomerase (Figure 1) for conversion of IPP to DMAPP (Clastre et al., 2007). There is a *C. parvum* enzyme with CryptoDB (Heiges et al., 2006) gene ID *cgd4_2550* (GenBank ID XP_625843), which shares 27% and 24% sequence identity, respectively, with human FPPS and GGPPS (see multiple sequence alignment in Figure S1 available online). We expressed the recombinant form of this protein and measured its activity using four allylic substrates (DMAPP,

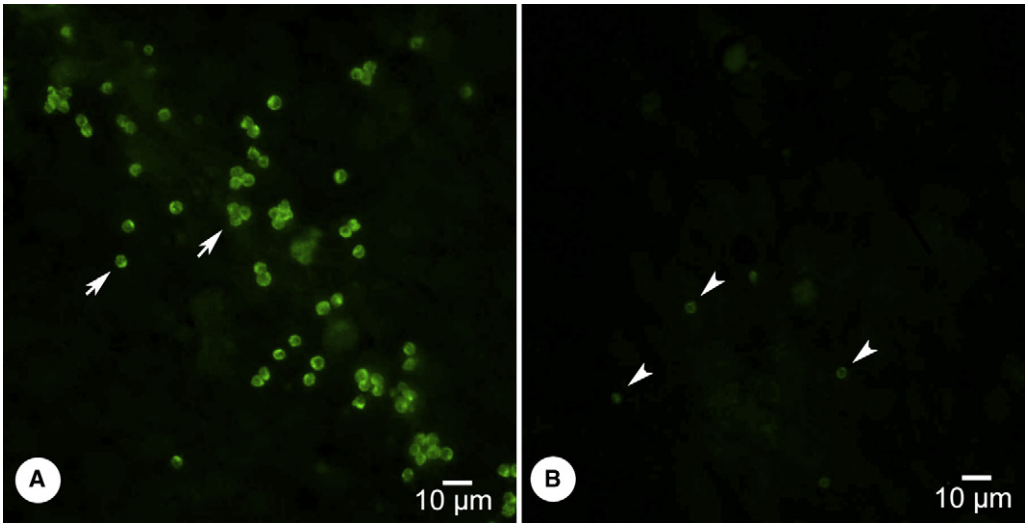

Figure 2. *C. parvum* Growth in MDCK Cells 48 h after Inoculation (PI) in the Presence of RIS
Immunofluorescence labeling of parasites utilized the *Cryptosporidium*-specific monoclonal antibody C3C3.
(A) Robust *C. parvum* growth in the presence of RIS at 1 μM (arrows).
(B) Substantial inhibition of parasite growth in the presence of RIS at 100 μM (reduced numbers of parasites, weaker antibody labeling, and smaller size of parasites [arrowheads]).

 ©2008 Elsevier Ltd All rights reserved

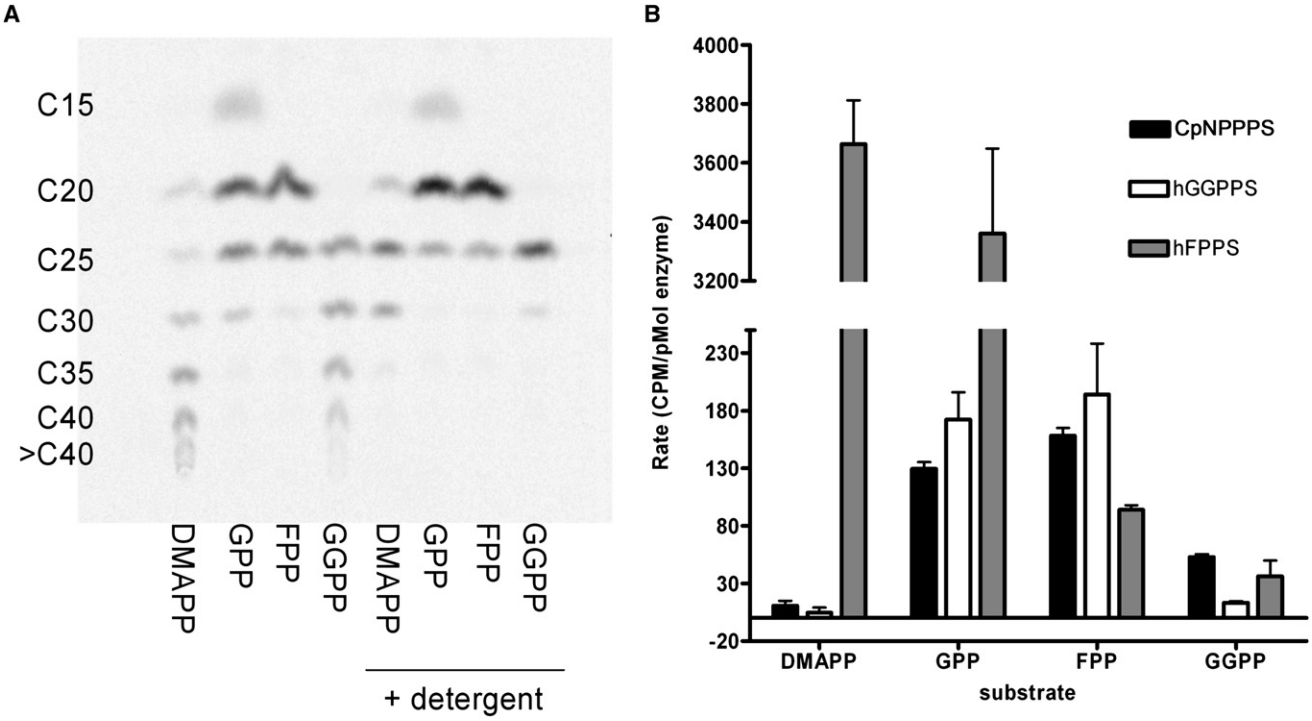

Figure 3. Comparative Biochemical Study of Human and Parasite Prenyl Synthases

(A) Reverse-phase TLC of the product distribution from the reaction of CpNPPPS with various substrates in the presence and absence of detergent.

(B) Rates of IPP incorporation into product by CpNPPPS, human GGPPS (hGGPPS), and human FPPS (hFPPS) with different substrates.

GPP, FPP, and GGPP) to evaluate its substrate and product specificities.

Product analysis by reverse-phase TLC revealed a wide range of polyprenyl chains (Figure 3A), regardless of the substrate used. With DMAPP as substrate, the rate of activity was low but still sufficient to show a roughly even distribution of products from C_{15} up to C_{45} (Table S1), with longer products occasionally observed (up to C_{55}). Nevertheless, the enzyme was clearly more active with GPP, FPP, and GGPP as substrates. When GGPP was the substrate, longer prenyl chains were also produced. Upon addition of detergent (Tween 20), all reactions lost their longest products. This was particularly noticeable with DMAPP or GGPP as the substrate (Figure 3A and Table S2). In both cases, the maximal chain length observed under these conditions was C_{35}, but the major products were C_{25} and C_{30}. Because of its versatility, we chose to call this enzyme *Cryptosporidium parvum* nonspecific polyprenyl pyrophosphate synthase (CpNPPPS).

The rate of IPP incorporation using the standard assay was barely measurable using DMAPP (Figure 3B), but we were able to determine the kinetic parameters of CpNPPPS with other substrates. The highest maximal velocity was obtained, in descending order (Table S3), with FPP (3.1 ± 0.1 nmol/min/nmol), GPP (1.4 ± 0.2 nmol/min/nmol), and GGPP (0.9 ± 0.1 nmol/min/nmol). Kinetic data fit the Michaelis-Menten model and showed the substrates to have similar K_M values between 0.8 and 0.95 μM (Table S3), comparable to the values previously determined for other prenyl synthases (Guo et al., 2007; Kavanagh et al., 2006a, 2006b). The K_M value for IPP was found to be 1.5 μM and also similar to other prenyl synthases (Kavanagh et al., 2006a, 2006b). We did not observe IPP-induced substrate inhibition with IPP concentrations up to 40 μM (data not shown). The *C. parvum* enzyme CpNPPPS had an IPP incorporation rate similar to human GGPPS, but was approximately 20-fold less active than human FPPS (Figure 3B).

Despite being a poor substrate for CpNPPPS, DMAPP does give a wide range of products (C_{15} to > C_{45}). Mechanistically, once this substrate begins the chain-elongation process, the DMAPP in solution cannot compete with the bound product/substrate. Although GGPP is a better substrate than DMAPP, the same holds true, where products greater than C_{45} can be detected. In the case of GPP and FPP, predominately products less than C_{30} are formed and longer-chain products are virtually undetectable. Overall, the presence of detergents leads to a decrease in product chain length, which can be attributed to the facilitation of product release in the presence of these large hydrophobic molecules in the bulk solvent. In contrast to CpNPPPS, human FPPS and GGPPS are both monofunctional and exclusively produce FPP and GGPP, respectively (Kavanagh et al., 2006a, 2006b).

Enzyme Inhibition: CpNPPPS Inhibited by N-BPs with Subnanomolar K_i Values

The potency and mode of binding for the three most potent anticryptospordial compounds from our experiments, namely RIS, ZOL, and IBAN, were evaluated for comparison with our results of growth inhibition in N-BPs-treated *C. parvum*-infected MDCK cells. As summarized in Table 2, the enzyme CpNPPPS was

 ©2008 Elsevier Ltd All rights reserved

Table 2. Enzyme Inhibition by N-BPs Found to Be Most Potent Anticryptoporidial Compounds

	IC_{50} (nM)	K_i^{app} (nM)	K_i (nM)
RIS	45.7 ± 2.6	4.6 ± 1.4	0.38 ± 0.12
ZOL	30.1 ± 1.1	0.60 ± 0.46	0.050 ± 0.038
IBAN	52.7 ± 7.6	19.4 ± 3.1	1.60 ± 0.26

found to be strongly inhibited by N-BPs and exhibited tight binding characteristics, with K_i and IC_{50} values in the same range as the enzyme concentration (e.g. $IC_{50,RIS}$ is 45.7 nM with the nominal enzyme assay concentration of 92 nM). The N-BPs also showed the time-dependent characteristics of slow binding. The initial inhibition of the enzyme by ZOL gives an IC_{50} value of 2.0 ± 0.2 μM and a K_i^{app} value of 2.2 ± 0.2 μM (see Figure S2 and Table 2 for other N-BPs). Upon preincubation of the enzyme and ZOL for 10 min, the IC_{50} decreased by approximately 70-fold. Lineweaver-Burke analysis of the inhibition of the enzyme by ZOL at different concentrations of one substrate while holding the second substrate constant shows that the N-BP is competitive for the allylic substrate (in this case FPP) and mixed (noncompetitive) for IPP (Figure S3). This effect was not taken into account in our calculation of the K_i^{app} value. With correction made for substrate competition, we obtained K_i values of 0.38 ± 0.12 nM, 0.05 ± 0.04 nM, and 1.60 ± 0.26 nM for RIS, ZOL, and IBAN, respectively. Clearly, all three drug compounds are highly potent inhibitors of the CpNPPPS enzyme, supporting the hypothesis that this is the mechanism of their anticryptosporidial effectiveness as seen in the MDCK cultures.

Crystallography: CpNPPPS in Structural Complexes with Clinically Relevant N-BPs

The structures of CpNPPPS-RIS (Protein Data Bank [PDB] ID: 2O1O), shown in Figure 4A, and CpNPPPS-ZOL (PDB ID: 2Q58) were determined to 2.42 Å (R = 18.6%, R_{free} = 21.3%) and 2.37 Å (R = 20.2%, R_{free} = 24.1%), respectively (Table 3). Nearly identical with rmds for C_α of < 0.5 Å, these structures reveal the enzyme to be a homodimer of subunits each made up of α helices joined by loops—a typical *trans*-prenyl synthase fold previously described for FPPS (Hosfield et al., 2004; Kavanagh et al., 2006b; Rondeau et al., 2006; Tarshis et al., 1994), GGPPS (Guo et al., 2007; Kavanagh et al., 2006a), and OPPS (Guo et al., 2005, 2004a). To be specific, the CpNPPPS-ZOL structure deviates by 1.56 Å and 2.67 Å, respectively, from the human FPPS-ZOL/IPP structure (PDB ID: 2F8Z) and apo *Thermotoga maritima* OPPS (PDB ID: 2AZL). The two highly conserved aspartate-rich allylic binding sites, namely FARM (first Asp-rich motif) and SARM (second Asp-rich motif), are located across an elongated central cavity enveloped by the helical core in each subunit, also as seen in other prenyl synthases (Chang et al., 2006; Kavanagh et al., 2006a, 2006b; Rondeau et al., 2006; Tarshis et al., 1994). The FARM sequence in CpNPPPS, specifically DDIMD, conforms to the DDXXD motif (X being any residue), whereas the first aspartate in the SARM is in fact an asparagine in this enzyme (NDVSD). Three Mg^{2+} ions are coordinated in an octahedral fashion through the Asp of the FARM, the Asp and Asn of the SARM, and the bisphosphonate oxygens of RIS and ZOL. Despite its inclusion in the crystallization condition, IPP was not found in either structure. Again, as in other prenyl synthases, the drug molecule (RIS in 2O1O, ZOL in 2Q58) is bound in CpNPPPS between helices α4, α8, and α9 (see CpNPPPS-ZOL in Figure 4B and CpNPPPS-RIS in Figure 4C). Key residues on each protein molecule interacting with it include the carbonyl of Lys226 and the O_χ of Thr227 (residue numbering based on sequence in CryptoDB gene record *cgd4_2550*) in a manner found in Saccharomyces *cerevisiae* GGPPS (for ZOL and minodronate) (Hosfield et al., 2004; Kavanagh et al., 2006b; Rondeau et al., 2006; Guo et al., 2007).

Variations among prenyl synthases in the chain length determination (CLD) region hold the key to their substrate preference. In enzymes that produce only FPPS, the chain-elongation cavity is delimited by two bulky residues (FF) four or five amino acids upstream from the FARM (Ohnuma et al., 1996a, 1996b; Tarshis et al., 1996). In GGPPS, which has no bulky residues upstream of the FARM, the triad of Leu67, Tyr107, and His139 is implicated in the CLD (Chang et al., 2006; Guo et al., 2007; Kloer et al., 2006). In OPPS from *T. maritima*, Phe132 has been shown to seal the larger chain-elongation cavity (Guo et al., 2004b) necessary for the C_{40} product. The new CpNPPPS enzyme lacks both the phenylalanine tandem in FPPS and the GGPPS triad. In their places are a less bulky (^{126}LI^{127}) pair and a smaller and more flexible triad of Ile123-Lys163-Val197. This relatively unencumbered cavity can accommodate a large array of substrates, products, and inhibitors, as visualized in Figure 5.

Despite its significantly larger active site, our crystallographic structures reveal that the typical binding of small N-BPs in the allylic binding site of prenyl synthases is preserved in CpNPPPS. This is not the only mechanism of inhibition of prenyl synthases, however, as shown in the inhibitor binding sites described for *S. cerevisiae* GGPPS and the inhibitory binding of GGPP in human GGPPS. Figure 5 shows some of the alternative possibilities for inhibitor binding in CpNPPPS based on previous work including: (1) the bisphosphonate moiety bound in the allylic binding site and extended into the hydrophobic pocket typically occupied by the growing isoprenyl chain (Figures 5A and 5C); (2) the bisphosphonate moiety bound in the allylic binding site where the remainder of the inhibitor is large and extends into the novel GGPP inhibitor site identified in human GGPPS (Figure 5F); (3) the bisphosphonate moiety bound in the homoallylic IPP binding site and the inhibitor side chain extending into the novel GGPP inhibitor site (Figure 5D); and (4) the diphosphate bound in the IPP site and the isoprenyl chain extending into the typical hydrophobic pocket occupied by the growing isoprenyl chain (Figure 5E).

Unique Isoprenoid Pathway in *Cryptosporidium* Offers Mechanism of Anticryptosporidial Action

Although humans have two distinct monofunctional enzymes to respectively produce FPP and GGPP, this is not the case in all organisms. For example, there are two reported archaeal enzymes that yield both FPP and GGPP in a temperature-dependent manner (Chen and Poulter, 1993; Fujiwara et al., 2004; Tachibana et al., 2000). In *Plasmodium* parasites, there is only one enzyme homologous by sequence to both human FPPS and GPPS; it produces strictly GGPP in biochemical assays (data not shown). Toxoplasma *gondii* FPPS produces a detectable but unquantified amount of GGPP in addition to the dominant

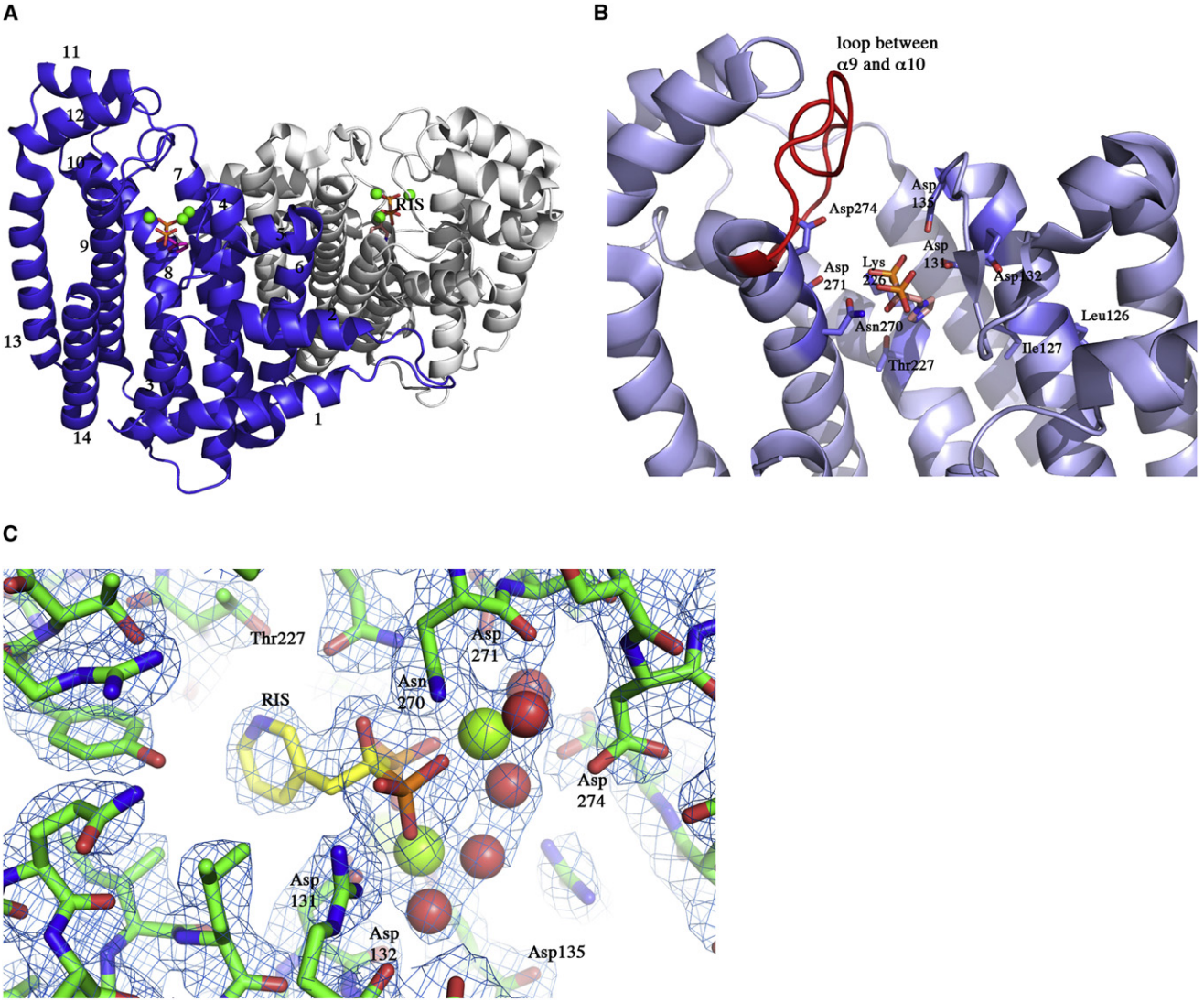

Figure 4. CpNPPPS Structures

(A) Overall view of CpNPPPS dimer with RIS bound. Helices are numbered in the blue subunit and risedronate is labeled in the white subunit.

(B) Active site from structure of CpNPPPS with ZOL bound (2Q58). The three aspartate residues of the FARM motif are shown (Asp131, Asp132, Asp135), as are Asn270, Asp 271, and Asp274 from the SARM. Also shown are the other conserved residues that interact with ZOL - ^{226}KT^{227}, and the CLD dyad of ^{126}LI^{127}. Residue numbering is based on sequence from the CryptoDB gene record *cgd4_2550*. (C) Electron density in risedronate-binding area with key residues in FARM and SARM showing. Water molecules are in red and magnesium ions are in green.

FPP product in the presence of high substrate concentrations and at long reaction times (Ling et al., 2007). Both *Plasmodium* and *Toxoplasma* employ the MEP pathway to manufacture IPP and DMAPP as substrates for these enzymes. In contrast, genomic analysis indicates the presence of neither the mevalonate nor the MEP pathway in *Cryptosporidium*. However, there is genomic evidence of enzymes involved in production of long-chain pyrophosphates, including a putative long-chain fatty acyl diphosphate synthase (CryptoDB gene ID *cgd7_3730*) and a putative long-chain *cis*-prenyl synthase, undecaprenyl pyrophosphate synthase (*cgd4_1510*). Further downstream, farnesyl tranferase (FTase) (*cgd6_2510*) has been implicated in presqualene diphosphate synthesis and might be capable of catalyzing the production of squalene from FPP and NADPH, α-subunit of Rab geranylgeranyl transferase (GGTase, *cgd7_5300*), 2 β-subunit of Rab GGTaseβ (*cgd6_1750*), Rab GGTaseβ1 (*cgd3_2350*), GGTaseβ (*cgd1_1980*), and UbiA prenyltransferase (*cgd3_2460*). Clearly, the parasite has the machinery to utilize isoprenoids for myriad functions, but it has not yet divulged its means to produce the requisite building blocks. Although there might be other novel enzymes that perform this function, the enzymatic versatility of CpNPPPS in vitro supports the possibility of a salvage pathway, possibly enabling the parasite to use whatever short- to medium-chain isoprenoids available from the host to manufacture longer products. In either case, the *Cryptosporidium* isoprenoid pathway is entirely different from what has been previously observed in all other organisms.

 ©2008 Elsevier Ltd All rights reserved

Table 3. Data Processing and Refinement Statistics

Protein Data Bank Code	2Q58	2O1O
Crystal		
Space group	$P3_1$	$P3_1$
Unit cell	a = b = 104.8Å c = 78.5Å $\alpha = \beta = 90°$, $\gamma = 120°$	a = b = 101.8Å c = 75.3Å $\alpha = \beta = 90°$, $\gamma = 120°$
Solvent content (%)	53	53
Matthews coefficient (Å ^{3}/Da)	2.6	2.6
No. of molecules in asymmetric unit	2	2
Data collection		
Wavelength (Å)	1.5418	1.5418
Resolution (Å)	50.0-2.2	50.0-2.42
Unique reflections	44405	32655
Redundancy	5.6	5.0
Completeness (%)	99.8	100
I/(I)	34.1	29.7
R_{merge} (%)	3.8	4.6
Refinement		
Resolution (Å)	50.0-2.37	50.0-2.42
Completeness (%)	94.9	94.9
Unique reflections	33571	31541
R_{all} (%)	20.2	18.6
R_{free} (%)	24.1	21.3
Number of protein atoms	5313	5310
Number of water molecules	48	28
B factor from Wilson plot (Å^2)	66	53
Average B factor (Å^2)	60	57
Ramachandran plot[a]		
Most favored regions (%)	82.7	86.7
Additional allowed regions (%)	15.7	12.5
Generously allowed regions (%)	1.0	0.5
Disallowed regions (%)	0.6	0.3

The crystal structure of human FDPS (PDB code: 1YV5), with all residues converted to alanine, was used as a search model. The twinning did not affect structure solution; and the fitted molecular replacement model was extended automatically with RESOLVE (Terwilliger, 2002) and rebuilt manually with COOT (Emsley and Cowtan, 2004). The twinning matrix (1 0 0 −1 −1 0 0 0 −1) and twin fraction (0.39) were determined by The Merohedral Crystal Twinning Server (http://nihserver.mbi.ucla.edu/Twinning/; Yeates, 1997); and detwinned data were generated. For map calculation, all data from the 50.0-2.2Å range were included, but because of very weak data in the highest-resolution shell, the high-resolution limit for refinement was set to 2.37Å. Initial refinement against the detwinned data was performed with REFMAC (Murshudov et al., 1997). Refinement with REFMAC converged with R and R_{free} equal to 27% and 34%, respectively. At this point the original data were used again and further refinement was carried out with SHELXL. The twinning fraction was refined to 0.45. The final refined model and the structure factors were deposited to the PDB under the accession code 2Q58 and were used as a starting model for molecular replacement of the complex with RIS. For the second crystal the initial twinning fraction, as determined by the Merohedral Crystal Twinning Server, was equal to 0.44 and increased to 0.49 when SHELXL was used for refinement. The final model of CpNPPPS in complex with RIS, and its structure factors, was deposited to the PDB under the accession code 2O1O.

[a] Ramachandran plots were generated with PROCHECK.

SIGNIFICANCE

Currently, drug treatment for cryptosporidiosis revolves around three different strategies that are also used in combination: nonspecific antimicrobial drugs, immunotherapy (for the immunocompromised), and symptomatic treatment with antidiarrheals, with none proven to be adequate (Mead, 2002). Without any validated drug targets and candidates on the horizon, an effective therapeutic solution appears a long way off. The use of bisphosphonates might be a study in opportunistic therapy for at least three main reasons. First, because a number of compounds in this family are drugs in clinical use with well-known pharmacokinetics, there is potential to accelerate the preclinical investigations necessary before testing these compounds in cryptosporidiosis patients. Second, we identified three potent anticryptosporidials out of seven N-BPs tested. This provides the impetus to study other bisphosphonates to identify candidates with an optimal profile in potency and pharmacokinetics, without further chemical development. Finally, whereas bisphosphonates' poor bioavailability might make them unsuitable for many infectious diseases, they could be ideal candidates for cryptosporidiosis treatment because the parasites congregate in the epithelial cells of the gastrointestinal lumen (Lin, 1996) and therefore do not require drugs to be transported through the blood system.

EXPERIMENTAL PROCEDURES

Reagents

All seven compounds used in this study—risedronate, zoledronate, alendronate, pamidronate, NE10790 and NE58051—were provided by Procter & Gamble Pharmaceuticals (Cincinnati, OH).

C. parvum Isolate for In Vitro Cultivation Studies

C. parvum oocysts (IOWA isolate) were generated in newborn Holstein bull calves and stored at 4°C in 2.5% (w/v) aqueous potassium dichromate (Arrowood and Sterling, 1987). Oocysts were purified from calf stool by sieving through stainless steel sieves, followed by discontinuous sucrose gradient and cesium chloride shelf gradient methods as previously described (Arrowood and Donaldson, 1996).

C. parvum In Vitro Cultivation Assay

Purified oocysts were diluted in UltraCULTURE synthetic culture medium (Lonza Group Ltd., Switzerland) and inoculated onto confluent MDCK cells in 2-well coverslip culture chambers (Nunc, Inc., Naperville, IL) and incubated at 37°C in a 5% CO_2 incubator. Oocyst inocula typically contained 500–2000 oocysts/mm^2 (~1 × 10^5/chamber). After 3 hr (to allow excystation and sporozoite invasion), the medium was removed, the monolayer was washed gently with PBS (to remove unattached parasites), fresh growth medium was replaced (with or without test compounds), and the culture chambers were incubated for a total of 48 hr (Arrowood et al., 1994). In each experiment, two replicates were prepared for each concentration of the test compounds.

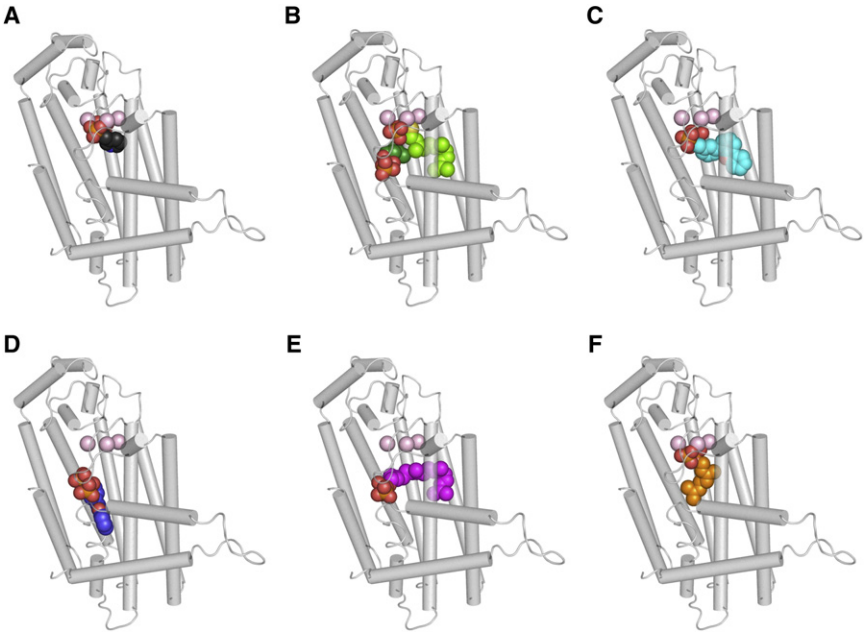

Figure 5. Predicted Binding of Substrates, Substrate Analogs, Products, and Inhibitors to CpNPPPS

Each image is created using WinCoot SSM Superpose by superimposing the respective structure and its associated ligand over CpNPPPS and displaying the resulting ligand orientated within the CpNPPPS-RIS structure. Visual inspection revealed no obvious interference of the ligand with the CpNPPPS structure. The Mg^{2+} ions from the CpNPPPS-RIS structure are shown in pink; the oxygens of the phosphate moieties are shown in red.

(A) RIS (black), PDB ID: 2O1O.

(B) IPP (dark green), FsPP (light green), PDB ID: 2E8T.

(C) BP629 in allylic site (light blue), PDB ID: 2E93.

(D) BP629 in IPP site (dark blue), PDB ID: 2E8T.

(E) GGPP in IPP site and across to FPP site (bright pink), PDB ID: 2E8V.

(F) GGPP in "inhibitor" site (orange), PDB ID: 2FVI.

Immunofluorescent Assay of Parasite Development

Cultures were fixed with Bouin's solution, decolorized with 70% ethanol, blocked with PBS supplemented with 0.1% bovine serum albumin (PBS/BSA, 30 min at room temperature [RT]), and labeled with a *Cryptosporidium*-specific monoclonal antibody labeled with fluorescein isothiocyanate (C3C3-FITC) or with neat C3C3 hybridoma supernatant (60 min at RT). Chambers incubated with unlabeled antibody were subsequently labeled (60 min at RT) with fluorescein-conjugated goat anti-mouse immunoglobulin (Zymed Laboratories Inc., San Francisco, CA). Labeled cell cultures were washed with PBS/BSA, overlayed with two drops of a glycerol-based mounting medium (with fluorescence anti-quenching agent), coverslipped, and stored at 4°C until examined (Arrowood, 2002).

Culture chambers were examined using epifluorescence at 100X magnification on a Zeiss Axiovert 200 microscope (Carl Zeiss Microimaging, Inc., Thornwood, NY). Seventy-two adjacent video frames (1388 × 1040 pixels) were digitized from each culture chamber (treatment replicate) with a Zeiss AxioCam HRm camera utilizing Zeiss AxioVision software. Life cycle stages were identified by reactivity with monoclonal antibody and by morphology (size and shape). Developing meronts and gamonts (~3–5 μm) were enumerated for each treatment chamber replicate with assistance from freeware image analysis software (ImageJ, NIH, Bethesda, MD) as number/mm^2 (Arrowood, 2002).

Parasite counts in treated chambers were compared with control chambers, inhibition was calculated, and IC_{50} values were determined by median effect analysis using CalcuSyn software (Biosoft, Cambridge, UK) (Chou, 2006).

Toxicity Assay

Bisphosphonate compounds were evaluated for toxicity using a tetrazolium salt-based assay (CellTiter 96, Promega Corp., Madison, WI) in MDCK and HCT-8 cells under conditions equivalent to those used for parasite culture.

Expression and Crystallography

An *N*-terminal truncation of cgd4_2550 (GenBank Accession: XP_625843) from E38-L384 with an N-terminal His_6-tag and TEV cleavage site (MGSSHHHHHHSSGRENLYFQ*G) was cloned, expressed using the Lex bioreactor system (Harbinger Biotechnology and Engineering Corp., Markham, Ontario, Canada), and purified as previously described (Vedadi et al., 2007). Purified CpNPPPS was crystallized using the hanging drop vapor diffusion method in a VDXm plate with 350 μl mother liquor at 18°C. Protein solution (1.5 μl of 10 mM RIS or ZOL, 10 mM IPP, and 10 mM $MgCl_2$) was mixed with the reservoir solution (1.5 μl of 1.6 M $(NH_4)_2SO_4$, 10 mM $MgCl_2$, and 100 mM HEPES, pH 7.5). Crystals appeared after 4–5 weeks. Diffraction data were collected using a Rigaku FR-E Superbright generator equipped with a Rigaku HTC image plate detector.

Enzymatic Assays

CpNPPPS was assayed using the method of Reed and Rilling with some modifications (Reed and Rilling, 1975). For the kinetic analysis, 400 ng (9.2 pmol) purified CpNPPPS was assayed in 100 μl buffer (50 mM Tris [pH 7.7], 2 mM $MgCl_2$, 1 mM TCEP, and 5 μg/ml BSA). The concentrations of GPP and IPP (^{14}C-IPP, 400 KBq/μmol) were typically 0.05 to 20 μM. The remainder of the assay was completed as described elsewhere (Kavanagh et al., 2006a). For inhibition experiments, 10 μl 10x N-BP was added to each assay; and to allow for any slow binding inhibition the enzyme was preincubated with the inhibitor in a total volume of 80 μl. After 10 min, 20 μl of a substrate mixture containing GPP and IPP (^{14}C-IPP, 400 KBq/μmol) was added to start the reaction (giving 100 μl total volume and 10 μM substrate). Assays were carried out at 37°C and subsequently terminated, extracted, and analyzed as described previously (Kavanagh et al., 2006a). Preincubation of enzyme and inhibitor experiments showed tight binding characteristics, so data were evaluated as detailed earlier (Kavanagh et al., 2006b). Analysis of the reaction products was completed using reverse-phase TLC (Fujii et al., 1982). Briefly, the ^{14}C-labeled enzyme products were dephosphorylated and separated on a C_{18} reverse-phase TLC plate (Analtech) using 3:1 acetone:water. The plate was then dried and imaged using a Storm 860 phosphor imager (GE Healthcare). VisionWorksLS software was used for the calculation of the relative yields for the isoprenoid products, and results were corrected for the amount of radioactivity incorporated into each product.

Crystallographic Data Processing, Structure Solution, and Refinement

Datasets were processed with HKL-2000 (Otwinowski and Minor, 1997). The protein crystallized in space group $P3_1$ in both crystals; and both crystals could be classified as partial merohedral twins. The structure of CpNPPPS-ZOL was solved by molecular replacement using MOLREP (Vagin and Teplyakov, 1997) as implemented in CCP4 (CCP4, 1994). The twinning did not affect structure solution; and the fitted molecular replacement model was extended automatically with RESOLVE (Terwilliger, 2002) and rebuilt manually with COOT (Emsley and Cowtan, 2004). The twinning matrix (h, -h-k, -l) and twin fraction (0.39) were determined by The Merohedral Crystal Twinning Server (http://nihserver.mbi.ucla.edu/Twinning/; Yeates, 1997). The final refined model and the structure factors were deposited to the PDB under the accession code 2Q58 and were used as a starting model for molecular replacement of the complex with RIS.

 ©2008 Elsevier Ltd All rights reserved

The final model of CpNPPPS-RIS (twin fraction 0.45) and its structure factors were deposited to the PDB with accession code 2O1O. Both structures were validated using PROCHECK (Laskowski et al., 1993), and MOLPROBITY (Lovell et al., 2003). Data collection and refinement statistics for both structures are summarized in Table 3.

SUPPLEMENTAL DATA

Supplemental Data include three tables and three figures and are available with this article online at http://www.cell.com/chemistry-biology/supplemental/S1074-5521(08)00448-1.

ACKNOWLEDGMENTS

The authors would like to acknowledge the Structural Genomics Consortium (SGC), Jocelyne Lew for the cloning of CpNPPPS, Helen Ren for large scale expression, and Heping Zheng for correcting the Ramachandran outliers of CpNPPPS-ZOL. The BL21(DE3)R3-pRARE2 strain of *Escherichia coli* used came from Opher Gileadi of the SGC at the University of Oxford. The SGC is a registered charity (# 1097737) that receives funds from the Canadian Institutes for Health Research, the Canadian Foundation for Innovation, Genome Canada through the Ontario Genomics Institute, GlaxoSmithKline, the Knut and Alice Wallenberg Foundation, the Ontario Innovation Trust, the Ontario Ministry for Research and Innovation, Merck & Co. Inc., the Novartis Research Foundation, the Petrus and Augusta Hedlund's Foundation, the Swedish Agency for Innovation Systems, the Swedish Foundation for Strategic Research, and the Wellcome Trust. This research was also supported by funds from the McLaughlin Centre of Molecular Medicine. The methodological part of this work was also supported in part by US NIH grant GM074942.

Received: March 20, 2008
Revised: September 30, 2008
Accepted: October 6, 2008
Published: December 19, 2008

REFERENCES

Arrowood, M.J. (2002). In vitro cultivation of *Cryptosporidium* species. Clin. Microbiol. Rev. *15*, 390–400.

Arrowood, M.J. (2007). In Vitro Cultivation. In *Cryptosporidium* and Cryptosporidiosis, Second Edition, R. Fayer and L. Xiao, eds. (Boca Raton, FL: CRC Press), pp. 499–525.

Arrowood, M.J., and Donaldson, K. (1996). Improved purification methods for calf-derived *Cryptosporidium parvum* oocysts using discontinuous sucrose and cesium chloride gradients. J. Eukaryot. Microbiol. *43*, 89S.

Arrowood, M.J., and Sterling, C.R. (1987). Isolation of *Cryptosporidium* oocysts and sporozoites using discontinuous sucrose and isopycnic Percoll gradients. J. Parasitol. *73*, 314–319.

Arrowood, M.J., Xie, L.T., and Hurd, M.R. (1994). In vitro assays of maduramicin activity against *Cryptosporidium parvum*. J. Eukaryot. Microbiol. *41*, 23S.

Bergstrom, J.D., Bostedor, R.G., Masarachia, P.J., Reszka, A.A., and Rodan, G. (2000). Alendronate is a specific, nanomolar inhibitor of farnesyl diphosphate synthase. Arch. Biochem. Biophys. *373*, 231–241.

Berkman, D.S., Lescano, A.G., Gilman, R.H., Lopez, S.L., and Black, M.M. (2002). Effects of stunting, diarrhoeal disease, and parasitic infection during infancy on cognition in late childhood: a follow-up study. Lancet *359*, 564–571.

CCP4. (1994). The CCP4 suite: programs for protein crystallography. Acta Crystallogr. D Biol. Crystallogr. *50*, 760–763.

Chang, T.H., Guo, R.T., Ko, T.P., Wang, A.H.J., and Liang, P.H. (2006). Crystal structure of type-III geranylgeranyl pyrophosphate synthase from *Saccharomyces cerevisiae* and the mechanism of product chain length determination. J. Biol. Chem. *281*, 14991–15000.

Chen, A., and Poulter, C.D. (1993). Purification and characterization of farnesyl diphosphate/geranylgeranyl diphosphate synthase: a thermostable bifunctional enzyme from *Methanobacterium thermoautotrophicum*. J. Biol. Chem. *268*, 11002–11007.

Chou, T.C. (2006). Theoretical basis, experimental design, and computerized simulation of synergism and antagonism in drug combination studies. Pharmacol. Rev. *58*, 621–681.

Clastre, M., Goubard, A., Prel, A., Mincheva, Z., Viaud-Massuart, M.C., Bout, D., Rideau, M., Velge-Roussel, F., and Laurent, F. (2007). The methylerythritol phosphate pathway for isoprenoid biosynthesis in coccidia: presence and sensitivity to fosmidomycin. Exp. Parasitol. *116*, 375–384.

Delmas, P.D. (2002). Treatment of postmenopausal osteoporosis. Lancet *359*, 2018–2026.

Emsley, P., and Cowtan, K. (2004). COOT: model-building tools for molecular graphics. Acta Crystallogr. D Biol. Crystallogr. *60*, 2126–2132.

Dunford, J.E., Thompson, K., Coxon, F.P., Luckman, S.P., Hahn, F.M., Poulter, C.D., Ebetino, F.H., and Rogers, M.J. (2001). Structure-activity relationships for inhibition of farnesyl diphosphate synthase in vitro and inhibition of bone resorption in vivo by nitrogen-containing bisphosphonates. J. Pharmacol. Exp. Ther. *296*, 235–242.

Fisher, J.E., Rodan, G.A., and Reszka, A.A. (2000). In vivo effects of bisphosphonates on the osteoclast mevalonate pathway. Endocrinology *141*, 4793–4796.

Fujii, H., Koyama, T., and Ogura, K. (1982). Efficient enzymatic hydrolysis of polyprenyl pyrophosphates. Biochim. Biophys. Acta *712*, 716–718.

Fujiwara, S., Yamanaka, A., Hirooka, K., Kobayashi, A., Imanaka, T., and Fukusaki, E. (2004). Temperature-dependent modulation of farnesyl diphosphate/geranylgeranyl diphosphate synthase from hyperthermophilic archaea. Biochem. Biophys. Res. Commun. *325*, 1066–1074.

Guo, R.T., Cao, R., Liang, P.H., Ko, P.T., Chang, T.H., Hudock, M.P., Jeng, W.Y., Chen, C.K., Zhang, Y., Song, Y., et al. (2007). Bisphosphonates target multiple sites in both cis- and trans-prenyltransferases. Proc. Natl. Acad. Sci. USA *104*, 10022–10027.

Guo, R.T., Ko, T.P., Chen, A.P.C., Kuo, C.J., Wang, A.H.J., and Liang, P.H. (2005). Crystal structures of undecaprenyl pyrophosphate synthase in complex with magnesium, isopentenyl pyrophosphate, and farnesyl thiopyrophosphate: roles of the metal ion and conserved residues in catalysis. J. Biol. Chem. *280*, 20762–20774.

Guo, R.T., Kuo, C.J., Chou, C.C., Ko, T.P., Shr, H.L., Liang, P.H., and Wang, A.H. (2004a). Crystal structure of octaprenyl pyrophosphate synthase from hyperthermophilic *Thermotoga maritima* and mechanism of product chain length determination. J. Biol. Chem. *279*, 4903–4912.

Guo, R.T., Kuo, C.J., Ko, T.P., Chou, C.C., Liang, P.H., and Wang, A.H. (2004b). A molecular ruler for chain elongation catalyzed by octaprenyl pyrophosphate synthase and its structure-based engineering to produce unprecedented long chain trans-prenyl products. Biochemistry *43*, 7678–7686.

Heiges, M., Wang, H., Robinson, E., Aurrecoechea, C., Gao, X., Kaluskar, N., Rhodes, P., Wang, S., He, C.Z., Su, Y., et al. (2006). CryptoDB: a *Cryptosporidium* bioinformatics resource update. Nucleic Acids Res. *34*, D419–D422.

Hosfield, D.J., Zhang, Y., Dougan, D.R., Broun, A., Tari, L.W., Swanson, R.V., and Finn, J. (2004). Structural basis for bisphosphonate-mediated inhibition of isoprenoid biosynthesis. J. Biol. Chem. *279*, 8526–8529.

Kavanagh, K.L., Dunford, J.E., Bunkoczi, G., Russell, R.G.G., and Oppermann, U. (2006a). The crystal structure of human geranylgeranyl pyrophosphate synthase reveals a novel hexameric arrangement and inhibitory product binding. J. Biol. Chem. *281*, 22004–22012.

Kavanagh, K.L., Guo, K.D., Dunford, J.E., Wu, X.Q., Knapp, S., Ebetino, F.H., Rogers, M.J., Russell, R.G.G., and Oppermann, U. (2006b). The molecular mechanism of nitrogen-containing bisphosphonates as anti osteoporosis drugs. Proc. Natl. Acad. Sci. USA *103*, 7829–7834.

Kloer, D.P., Welsch, R., Beyer, P., and Schulz, G.E. (2006). Structure and reaction geometry of geranylgeranyl diphosphate synthase from *Sinapis alba*. Biochemistry *45*, 15197–15204.

Laskowski, R.A., MacArthur, M.W., Moss, D.S., and Thornton, J.M. (1993). Procheck: a program to check the stereochemical quality of protein structures. J. Appl. Crystallogr. *26*, 283–291.

Lin, J.H. (1996). Bisphosphonates: a review of their pharmacokinetic properties. Bone *18*, 75–85.

 ©2008 Elsevier Ltd All rights reserved

Ling, Y., Li, Z.H., Miranda, K., Oldfield, E., and Moreno, S.N. (2007). The farnesyl diphosphate/geranylgeranyl diphosphate synthase of *Toxoplasma gondii* is a bifunctional enzyme and a molecular target of bisphosphonates. J. Biol. Chem. *282*, 30804–30816.

Ling, Y., Sahota, G., Odeh, S., Chan, J.M.W., Araujo, F.G., Moreno, S.N.J., and Oldfield, E. (2005). Bisphosphonate inhibitors of *Toxoplasma gondii* growth: in vitro, QSAR, and in vivo investigations. J. Med. Chem. *48*, 3130–3140.

Liu, C.I., Liu, G.Y., Song, Y., Yin, F., Hensler, M.E., Jeng, W.Y., Nizet, V., Wang, A.H., and Oldfield, E. (2008). A cholesterol biosynthesis inhibitor blocks *Staphylococcus aureus* virulence. Science *319*, 1391–1394.

Lovell, S.C., Davis, I.W., Arendall, W.B., 3rd, de Bakker, P.I., Word, J.M., Prisant, M.G., Richardson, J.S., and Richardson, D.C. (2003). Structure validation by Calpha geometry: phi,psi and Cbeta deviation. Proteins *50*, 437–450.

Martin, M.B., Grimley, J.S., Lewis, J.C., Heath, H.T., 3rd, Bailey, B.N., Kendrick, H., Yardley, V., Caldera, A., Lira, R., Urbina, J.A., et al. (2001). Bisphosphonates inhibit the growth of *Trypanosoma brucei, Trypanosoma cruzi, Leishmania donovani, Toxoplasma gondii*, and *Plasmodium falciparum*: a potential route to chemotherapy. J. Med. Chem. *44*, 909–916.

Mead, J.R. (2002). Cryptosporidiosis and the challenges of chemotherapy. Drug Resist. Updat. *5*, 47–57.

Moreno, B., Bailey, B.N., Luo, S., Martin, M.B., Kuhlenschmidt, M., Moreno, S.N., Docampo, R., and Oldfield, E. (2001). (31)P NMR of apicomplexans and the effects of risedronate on *Cryptosporidium parvum* growth. Biochem. Biophys. Res. Commun. *284*, 632–637.

Murshudov, G.N., Vagin, A.A., and Dodson, E.J. (1997). Refinement of macromolecular structures by the maximum-likelihood method. Acta Crystallogr. D Biol. Crystallogr. *53*, 240–255.

Ohnuma, S., Hirooka, K., Hemmi, H., Ishida, C., Ohto, C., and Nishino, T. (1996a). Conversion of product specificity of archaebacterial geranylgeranyl-diphosphate synthase - Identification of essential amino acid residues for chain length determination of prenyltransferase reaction. J. Biol. Chem. *271*, 18831–18837.

Ohnuma, S., Nakazawa, T., Hemmi, H., Hallberg, A.M., Koyama, T., Ogura, K., and Nishino, T. (1996b). Conversion from farnesyl diphosphate synthase to geranylgeranyl diphosphate synthase by random chemical mutagenesis. J. Biol. Chem. *271*, 10087–10095.

Otwinowski, Z., and Minor, W. (1997). Processing of X-ray diffraction data collected in oscillation mode. In Methods in Enzymology, Volume 276: Macromolecular Crystallography, Part A, C.W. Carter, Jr. and R.M. Sweet, eds. (New York: Academic Press), pp. 307–326.

Perkins, M.E., Wu, T.W., and Le Blancq, S.M. (1998). Cyclosporin analogs inhibit in vitro growth of *Cryptosporidium parvum*. Antimicrob. Agents Chemother. *42*, 843–848.

Reed, B.C., and Rilling, H.C. (1975). Crystallization and Partial Characterization of Prenyltransferase from Avian Liver. Biochemistry *14*, 50–54.

Ricci, K.A., Girosi, F., Tarr, P.I., Lim, Y.W., Mason, C., Miller, M., Hughes, J., von Seidlein, L., Agosti, J.M., and Guerrant, R.L. (2006). Reducing stunting among children: the potential contribution of diagnostics. Nature *444* (*Suppl 1*), 29–38.

Rogers, M.J., Gordon, S., Benford, H.L., Coxon, F.P., Luckman, S.P., Monkkonen, J., and Frith, J.C. (2000). Cellular and molecular mechanisms of action of bisphosphonates. Cancer *88*, 2961–2978.

Rondeau, J.M., Bitsch, F., Bourgier, E., Geiser, M., Hemmig, R., Kroemer, M., Lehmann, S., Ramage, P., Rieffel, S., Strauss, A., et al. (2006). Structural basis for the exceptional in vivo efficacy of bisphosphonate drugs. ChemMedChem *1*, 267–273.

Sanz-Rodriguez, C.E., Concepcion, J.L., Pekerar, S., Oldfield, E., and Urbina, J.A. (2007). Bisphosphonates as inhibitors of *Trypanosoma cruzi* hexokinase: kinetic and metabolic studies. J. Biol. Chem. *282*, 12377–12387.

Savioli, L., Smith, H., and Thompson, A. (2006). Giardia and *Cryptosporidium* join the "Neglected Diseases Initiative". Trends Parasitol. *22*, 203–208.

Smith, H.V., and Corcoran, G.D. (2004). New drugs and treatment for cryptosporidiosis. Curr. Opin. Infect. Dis. *17*, 557–564.

Tachibana, A., Yano, Y., Otani, S., Nomura, N., Sako, Y., and Taniguchi, M. (2000). Novel prenyltransferase gene encoding farnesylgeranyl diphosphate synthase from a hyperthermophilic archaeon, Aeropyrum pernix: molecularevolution with alteration in product specificity. Eur. J. Biochem. *267*, 321–328.

Tarshis, L.C., Proteau, P.J., Kellogg, B.A., Sacchettini, J.C., and Poulter, C.D. (1996). Regulation of product chain length by isoprenyl diphosphate synthases. Proc. Natl. Acad. Sci. USA *93*, 15018–15023.

Tarshis, L.C., Yan, M.J., Poulter, C.D., and Sacchettini, J.C. (1994). Crystal structure of recombinant farnesyl diphosphate synthase at 2.6-Angstrom resolution. Biochemistry *33*, 10871–10877.

Terwilliger, T.C. (2002). Automated structure solution, density modification and model building. Acta Crystallogr. D Biol. Crystallogr. *58*, 1937–1940.

Vagin, A., and Teplyakov, A. (1997). MOLREP: an automated program for molecular replacement. J. Appl. Crystallogr. *30*, 1022–1025.

van Beek, E., Pieterman, E., Cohen, L., Lowik, C., and Papapoulos, S. (1999). Nitrogen-containing bisphosphonates inhibit isopentenyl pyrophosphate isomerase/farnesyl pyrophosphate synthase activity with relative potencies corresponding to their antiresorptive potencies in vitro and in vivo. Biochem. Biophys. Res. Commun. *255*, 491–494.

Vedadi, M., Lew, J., Artz, J., Amani, M., Zhao, Y., Dong, A., Wasney, G.A., Gao, M., Hills, T., Brokx, S., et al. (2007). Genome-scale protein expression and structural biology of *Plasmodium falciparum* and related Apicomplexan organisms. Mol. Biochem. Parasitol. *151*, 100–110.

Yeates, T.O. (1997). Detecting and overcoming crystal twinning. In Methods in Enzymology, Volume 276: Macromolecular Crystallography, Part A, C.W. Carter, Jr. and R.M. Sweet, eds. (New York: Academic Press), pp. 344–358.

 ©2008 Elsevier Ltd All rights reserved